BL-2A/2013S2-002

Determining the impurity level positions in Ir-doped $SrTiO_3$ by HRPES

Seiji Kawasaki[1], Kazuto Akagi[2], Ryota Takahashi[1], Jun Yoshinobu[1], Fumio Komori[1], Koji Horiba[3], Hiroshi Kumigashira[3], Katsuya Iwashina[4], Akihiko Kudo[4], and Mikk Lippmaa[1*]
[1] Institute for Solid State Physics, University of Tokyo, Kashiwa 277-8581, Japan
[2] WPI-AIMR, Tohoku University, Sendai 980-8577, Japan
[3] Photon Factory, High Energy Accelerator Research Organization, Tsukuba 305-0801, Japan
[4] Faculty of Science, Tokyo University of Science, Tokyo 162-8601, Japan

Ir:$SrTiO_3$ has been reported to be a visible-light driven photocatalyst for water splitting. The photocatalytic activity of Ir:$SrTiO_3$ is strongly dependent on the valence of Ir; Ir^{4+}:$SrTiO_3$ is active for photoelectrochemical water oxidation but Ir^{3+}:$SrTiO_3$ is inert. The Ir impurity level positions are predicted to be one of the important factors for the photocarrier lifetime and transport. The impurity levels of Ir:$SrTiO_3$ were determined by high resolution photoemission spectroscopy (HRPES) at BL-2A. Ir^{4+} creates two impurity levels in the $SrTiO_3$ band gap region, where an unoccupied state at 0.8 eV below the conduction band and an occupied state at 0.8 eV above the valence band are formed. In contrast, Ir^{3+} creates an occupied impurity level at 1.6 eV below the conduction band. The impurity level which locates far from both valence and conduction bands generally works as a strong trap site for photocarriers, explaining that Ir^{3+}:$SrTiO_3$ does not show any photoresponse. Understanding the relationship between the electronic structure and the photocatalytic activity of photocatalysts leads us to develop more efficient photocatalytic activity.

1 Introduction

Photocatalytic and photoelectrochemical water splitting are promising ways for converting solar energy to chemical energy in the form of hydrogen [1-3]. Photocatalytic materials have been widely studied since the discovery of the water splitting effect on TiO_2 in the beginning of the 1970s [4]. To create efficient photocatalysts for solar water splitting, the ability to harness visible light, suitable band alignment with water redox potentials, and long-term stability in water are the most important factors. From the view point of water stability, oxides are generally more stable than silicon, sulfides, nitrides or other compound semiconductors. However, in most oxide semiconductors, the valence band (VB) is formed primarily by the oxygen 2*p* states that are located at +2.94 V vs. SHE [5] while the O_2/H_2O redox potential is at +1.23 V vs. SHE. Therefore, the number of oxide semiconductor candidates for solar water splitting is limited and careful materials design is required to obtain an efficient photocatalyst.

$SrTiO_3$ is a good starting point for photocatalyst design; it has a cubic perovskite structure with a band gap of 3.2 eV [6] and shows photocatalytic water splitting activity under ultraviolet (UV) light [7-9]. Chemical doping with anions and/or cations is a common technique to induce a visible-light response in a wide-gap material. [1] N, Cr, Rh, and Ir have been reported to be effective for this purpose in $SrTiO_3$ [10-14]. However, a general understanding of the effectiveness of the different dopant species for photocatalytic activity has not been achieved yet.

We have recently studied the relationship between the electronic structure and the photocatalytic activity of Rh^{4+}- and Rh^{3+}-doped $SrTiO_3$, showing the disadvantage of a mid-gap impurity level and the importance of hybridization between impurity levels and the valence band [15]. Rh^{4+}:$SrTiO_3$ shows low photocatalytic activity because Rh^{4+} forms an unoccupied mid-gap impurity level that is a strong recombination site for photocarriers. In contrast, Rh^{3+}:$SrTiO_3$ shows visible-light driven photocatalytic activity for the H_2-evolution reaction because Rh^{3+} only has a single occupied impurity level at the top of the VB where hybridization with the VB is possible.

In the present work, we focus on Ir:$SrTiO_3$ and investigate the relationship between the electronic structure and the photoelectrochemical properties of Ir:$SrTiO_3$. The results suggest that the Ir impurity level positions in the band gap of $SrTiO_3$ and the hybridization between the Ir donor level and the VB are crucial for obtaining a photocatalytic material with a high photoelectrochemical activity.

2 Experiment

Non-doped and Ir-doped $SrTiO_3$ powders were synthesized following the procedures used in earlier bulk photocatalyst work [10]. Ir(5%):$SrTiO_3$ epitaxial thin film samples were fabricated by pulsed laser deposition (PLD). The valence of Ir in $SrTiO_3$ was controlled by tuning the deposition condition; T = 700°C and $P(O_2) = 10^{-1}$ Torr was used for making a fully oxidized yellow Ir^{4+}:$SrTiO_3$ film, while T = 700°C and $P(O_2) = 10^{-6}$ Torr was used for making a reduced brown Ir^{3+}:$SrTiO_3$, similar to the case of Rh:$SrTiO_3$ [16]. Ir:$SrTiO_3$ films were deposited on double-side-polished $SrTiO_3$ (001) substrates to measure UV-Vis-NIR absorption spectra. Conductive Nb(0.05wt%):$SrTiO_3$ (001) substrates were used for Ir:$SrTiO_3$ film growth for preparing the PES samples in order to suppress the charging effect during the measurements. The film thickness of Ir:$SrTiO_3$ was 400 nm for UV-Vis-NIR spectra and 20 nm for PES spectra.

The electronic structure of $Ir^{4+/3+}$:$SrTiO_3$ was evaluated by optical absorption spectroscopy in ultraviolet, visible, and near infrared (UV-Vis-NIR) spectral ranges, first-

principles calculations, and HRPES. The UV-Vis-NIR absorption spectra were measured in transmittance mode for film samples or calculated from reflectance by the Kubelka-Munk method for powder samples. The occupied Ir 5*d* impurity level positions were determined with HRPES with a Scienta SES2002 electron analyzer using a synchrotron light source at Photon Factory BL-2A (High Energy Accelerator Research Organization, KEK).

The density of states (DOS) of non-doped and $Ir^{4+/3+}$(3.70 at.%)-doped $SrTiO_3$ were obtained by first-principles calculations using the VASP code [17, 18]. The HSE06 hybrid functional [19] was used to reproduce accurately the band gap width and the positions of the in-gap impurity levels. A 3 × 3 × 3 $SrTiO_3$ unit cell was used with one of the Ti^{4+} sites substituted by a Ir^{4+} ion, corresponding to a doping level of 3.70 atom %. The Ir^{3+}:$SrTiO_3$ system was modeled by introducing an additional electron with the same amount of positive background charge.

3 Results and Discussion

Figure 1 shows UV-Vis-NIR optical absorption spectra of non-doped and Ir(5%)-doped $SrTiO_3$ powder and film samples. The different Ir valence states in the films can be easily distinguished visually, as the films deposited at 700 °C and 10^{-1} Torr were yellow, while those grown at 10^{-6} Torr were brown. The absorption edge at 380 nm corresponds to the band gap excitation of $SrTiO_3$ (E_g = 3.2 eV) [6]. For fully oxidized films, grown at 10^{-1} Torr, the increase in absorption at wavelengths shorter than 600 nm includes two excitations; from the valence band (VB) to an unoccupied Ir^{4+} acceptor level, marked *B* in Figure 1 (b), and from the occupied Ir^{4+} donor level (*A*) to the conduction band (CB). The broad peak at 800 nm (1.55 eV) corresponds to a *d*–*d* transition (state *A* to *B*). On the other hand, the film deposited at 10^{-6} Torr only showed a broad absorption slope between 400 and 1000 nm. This absorption contains excitations from the Ir^{3+} donor level (*C*) to the CB in addition to the absorption features observed for the film deposited at 10^{-1} Torr because the films grown at low pressures contained a mixture of Ir 4+ and 3+ valence states (Ir^{4+} : Ir^{3+} = 28 : 72 was measured from Ir 4*f* core level XPS spectra).

To determine the Ir 5*d* impurity level positions in the band gap region of Ir:$SrTiO_3$, HRPES was performed using a synchrotron light source. Figure 2 shows valence band spectra of Ir(5%):$SrTiO_3$ films deposited at 700°C and either 10^{-1} or 10^{-6} Torr of oxygen, measured at photon energies hν = 600, 1000, and 1400 eV. The binding energy was referenced to the Au Fermi edge. The main components observed in the valence band region are attributed to bonding (O 2*p*-σ) and non-bonding O 2*p* (O 2*p*-π) orbitals at ~6 and ~4 eV binding energies, respectively [15, 20]. The contribution of Ir states to the valence band spectra cannot be easily seen due to an overlap with the oxygen 2*p* states. However, the photoexcitation cross-section ratio of Ir/O increases with the incident photon energy. A comparison of VB spectra taken at photon energies of 600, 1000, and 1400 eV can thus be used to separate the Ir contribution from the O 2*p* states. The difference spectra in Figure 2(b) were calculated by subtracting the hν = 600 eV spectrum from the hν = 1000 eV and hν = 1400 eV spectra, showing two peaks at ~8 eV and ~2 eV. The peak observed at the top of the VB at ~2 eV is assigned to the Ir 5*d* orbitals, while the peak at the bottom of the VB (~8 eV) corresponds to O 2*p*-σ orbitals hybridizing with Ir 5*d* states [21].

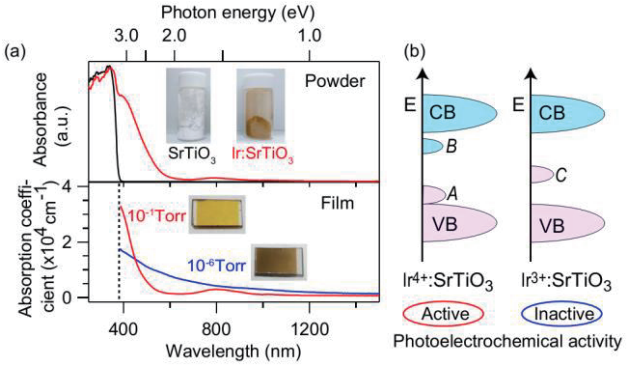

Fig. 1: (a) UV-Vis-NIR absorption spectra of non-doped $SrTiO_3$ and Ir(5%):$SrTiO_3$ powders and Ir(5%):$SrTiO_3$ films together with representative sample images. The film color changed systematically from yellow at 10^{-1} Torr to brown at 10^{-6} Torr. Absorption spectra of powder samples were obtained from diffuse reflectance data. The expected band structure for $Ir^{4+/3+}$:$SrTiO_3$ is shown in (b).

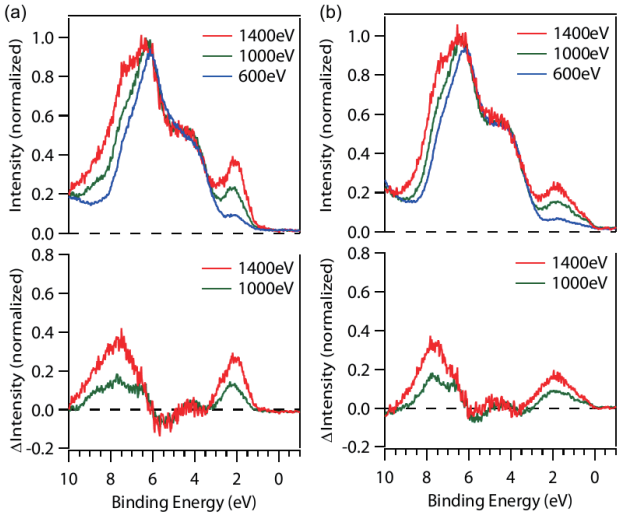

Fig. 2: Synchrotron X-ray photoelectron spectra of the VB of Ir(5%):$SrTiO_3$ films deposited at (a) 700°C, 10^{-1} Torr and (b) 700°C, 10^{-6} Torr. The photon energy was set at either 600, 1000 or 1400 eV. An increase of the Ir-related spectral components can be seen in the difference spectra measured at higher photon energies; the intensity increase is visualized by subtracting the hν = 600 eV data from the spectra taken at hν = 1000 and 1400 eV.

The Ir 5*d* spectral components close to the top of the VB, within the gap of the $SrTiO_3$ host material were deconvoluted to show the Ir^{4+} 5*d*, Ir^{3+} 5*d*, Ir metal 5*d*, and O 2*p*-π components, as shown in Figure 3. Ir^{3+} creates a donor level higher than Ir^{4+}, as shown in Figure 2(b). The

binding energy positions of Ir^{4+} 5*d* and Ir^{3+} 5*d* peaks are at 2.24 and 1.74 eV, respectively. The Ir metal contribution was calculated by including a thermally broadened Fermi-Dirac function because the VB spectrum of Ir-metal is nearly flat in the 0 to 6 eV binding energy range. [22] Exposure of the film surface to an intense synchrotron x-ray beam in ultra-high vacuum (UHV) resulted in moderate radiation damage, partially reducing Ir^{4+} to Ir^{3+} and Ir^{3+} to metallic Ir. Thus, the spectrum of the film deposited at 10^{-1} Torr has both Ir^{4+} and Ir^{3+} components in Figure 3, while only Ir^{4+} was observed for Ir 4*f* core level spectra by XPS with a laboratory X-ray source. Furthermore, the film deposited at 10^{-6} Torr has three components, corresponding to Ir^{4+}, Ir^{3+}, and metallic Ir.

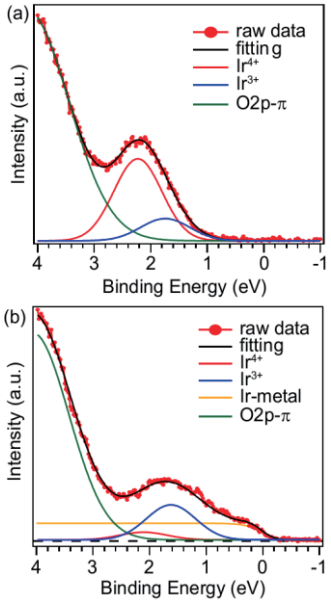

Fig.3: HRPES spectra of the VB of Ir(5%):$SrTiO_3$ films deposited at (a) 700°C, 10^{-1} Torr and (b) 700°C, 10^{-6} Torr. The photon energy was 1000 eV. Each raw spectrum (dotted line) is deconvoluted to Ir^{4+} 5*d* (red), Ir^{3+} 5*d* (blue), Ir metal 5*d* (orange), and O 2*p*-π (green) components. The fitting curve is shown in black.

The calculated total and partial density of states (PDOS) of Ir for $Ir^{4+/3+}$(3.7 at%):$SrTiO_3$ and non-doped $SrTiO_3$ are shown in Figure 4. The vertical scale for $Ir^{4+/3+}$:$SrTiO_3$ has been multiplied by 10. The Fermi level positions are marked by E_F in the plots. The calculation shows that two in-gap features related to the Ir 5*d* orbitals exist for Ir^{4+} substituting at the Ti^{4+} site in $SrTiO_3$, with peaks appearing ~0.5 eV higher than the top of the VB and ~0.8 eV below the bottom of the CB, labeled *A* and *B*, respectively. For Ir^{3+}, only a single in-gap level was found in the mid-gap region ~1.2 eV higher than the top of VB, labeled *C*. The *A*, *B*, and *C* states in Figure 4 correspond to the *A*, *B*, and *C* peaks in Figure 1 (b). It should be noted that all of these impurity levels are derived from Ir 5*d* t_{2g} states, and that state *B* is induced by the short-range Hartree-Fock exchange interaction in the HSE06 functional due to the existence of an unpaired electron at the Ir^{4+} (d^5) site. The Ir 5*d* e_g states are at a higher energy and overlap with the $SrTiO_3$ CB. Simulation using the GGA functional without considering the exchange interaction produces only a single impurity level in the gap region for Ir- and Rh-doped $SrTiO_3$ [23].

It should be noted that the impurity level positions of Ir:$SrTiO_3$ are similar to those of $Rh^{4+/3+}$:$SrTiO_3$ [15], and the difference between Rh and Ir doping is only seen as a shift of Ir impurity levels by ~0.5 eV higher than those of Rh in $SrTiO_3$. Rh and Ir are in the same group in the periodic table, but the Ir 5*d* impurity levels are systematically ~0.5 eV higher than those of the Rh 4d in the $SrTiO_3$ parent compound. At the bottom of the VB, at relative energies of −2 to −4 eV in Figure 4, Ir 5*d* and O 2*p* PDOS components overlap for both Ir^{4+}- and Ir^{3+}-doped samples, which corresponds to the increase of spectral intensity in the 7 to 9 eV binding energy range in Figure 2. The Ir 5*d* in-gap impurity levels and the O 2*p*-σ (O-Ir) lower VB states simulated by first-principles calculations are consistent with the experimental results obtained from UV-Vis-NIR absorption spectra and XPS measurements.

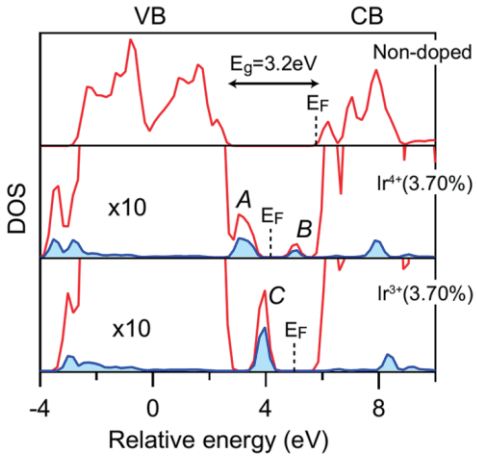

Fig.4: Density of states calculation results for non-doped $SrTiO_3$ and $Ir^{4+/3+}$(3.70%):$SrTiO_3$. The total DOS (red line) and PDOS of Ir (blue line) are shown for each sample. The vertical scale for $Ir^{4+/3+}$(3.70%):$SrTiO_3$ is multiplied by 10. The Ir^{4+} donor and acceptor levels are marked with *A* and *B*, respectively. The Ir^{3+} donor level is marked with *C*. E_F marks the calculated Fermi level positions.

The fact that Ir^{3+}:$SrTiO_3$ does not show any photoelectrochemical response, while Ir^{4+}:$SrTiO_3$ is active for water photo-oxidation, could be understood by considering the electronic structure. The impurity level which locates far from both VB and CB, like *C* state in Ir^{3+}:$SrTiO_3$, generally works as a strong trap site for photocarriers which accelerate photocarrier recombination, explaining that Ir^{3+}:$SrTiO_3$ does not show any photoresponse for water splitting reaction.

4 Conclusions

The impurity levels of Ir:$SrTiO_3$ were elucidated by UV-Vis-NIR and HRPES spectroscopic techniques with the support of first-principles calculations. Ir^{4+} creates two

impurity levels in the $SrTiO_3$ band gap region, where an unoccupied state at 0.8 eV below the CB and an occupied state at 0.8 eV above the VB are formed. In contrast, Ir^{3+} creates an occupied impurity level at 1.6 eV below the CB. An impurity level that is located far from both VB and CB edges generally works as a strong recombination center for photocarriers, explaining why Ir^{3+}:$SrTiO_3$ does not show any photoresponse. Understanding the relationship between the electronic structure and the photocatalytic activity of photocatalysts helps us to develop more efficient photocatalytic materials.

Acknowledgement

Computational resources were provided by the Supercomputer Center, Institute for Solid State Physics, University of Tokyo. WPI-Advanced Institute for Materials Research (WPI-AIMR), Tohoku University is supported by the World Premier International Research Center Initiative (WPI), MEXT, Japan.

References

[1] A. Kudo, and Y. Miseki, *Chem. Soc. Rev.* **38**, 253 (2009).
[2] X. Chen *et al.*, *Chem. Rev.* **110**, 6503 (2010).
[3] E. F. Osterloh, *Chem. Mater.* **20**, 35 (2008).
[4] A. Fujishima, and K. Honda, *Nature* **238**, 37 (1972).
[5] S. D. Scaife, *Solar Energy* **25**, 41 (1980).
[6] M. Cardona, *Phys. Rev.* **140**, A651 (1965).
[7] J. G. Mavroides *et al.*, *Appl. Phys. Lett.* **28**, 241 (1976).
[8] T, Watanabe *et al.*, *Bull. Chem. Soc. Jpn.* **49**, 355 (1976).
[9] M. S. Wrighton *et al.*, *J. Am. Chem. Soc.* **98**, 2774 (1976).
[10] R. Konta *et al.*, *J. Phys. Chem. B* **108**, 8992 (2004).
[11] H. Kato and A. Kudo, *J. Phys. Chem. B* **106**, 5029 (2002).
[12] T. Ishii *et al.*, *J. Photochem. Photobiol. A* **163**, 181 (2004).
[13] D. Wang *et al.*, *J. Phys. Chem. B* **110**, 15824 (2006).
[14] J. Wang *et al*., *J. Photochem. Photobiol. A* **165**, 149 (2004).
[15] S. Kawasaki *et al.*, *J. Phys. Chem. C* **116**, 24448 (2012).
[16] S. Kawasaki *et al.*, *Appl. Phys. Lett.* **101**, 033910 (2012).
[17] K. Kresse and J. Hafner, *Phys. Rev. B* **47**, 558 (1993).
[18] K. Kresse and J. Furthmuller, *Phys. Rev. B* **54**, 11169 (1996).
[19] J. Heyd *et al.*, *J. Chem. Phys.* **124**, 219906 (2006).
[20] T. Higuchi *et al.*, *Phys. Rev. B* **57**, 6978 (1998).
[21] J. M. Kahk *et al.*, *Phys. Rev. Lett*. **112**, 117601 (2014).
[22] D. E. Ibbotson *et al.*, *Surf. Sci*. **110**, 313 (1981).
[23] H. C. Chen *et al.*, *J. Phys. Chem. C* **116**, 7897 (2012).

Research Achievements (option)

1. A paper related to this study has been submitted to the Journal of Physical Chemistry.

* mlippmaa@issp.u-tokyo.ac.jp